Low-energy elastic electron scattering from ethylene: Elastic scattering and vibrational excitation

M. A. Khakoo, S. M. Khakoo, A. Sakaamini, B. A. Hlousek, L. R. Hargreaves, J. Lee, and R. Murase

Phys. Rev. A **93**, 012710 — Published 20 January 2016

DOI: 10.1103/PhysRevA.93.012710

LOW-ENERGY ELASTIC ELECTRON SCATTERING FROM ETHYLENE: ELASTIC SCATTERING AND VIBRATIONAL EXCITATION

M. A. Khakoo[1], S. M. Khakoo[2], A. Sakaamini[1], B. A. Hlousek[1], L. R. Hargreaves[1], J. Lee[3] and R. Murase[3]

[1] Department of Physics, California State University, Fullerton, CA 92831

[2] Department of Chemistry & Biochemistry, California State University, Fullerton, CA 92831

[3] Troy High School, 2200 Dorothy Lane, Fullerton, CA 92831

ABSTRACT: Normalized experimental differential and integral cross sections for elastic and vibrationally inelastic scattering of low-energy electrons from ethylene (C_2H_4) have been measured over a large number of incident electron energies and angles. The differential cross sections are measured at incident energies from 0.5 to 100 eV and scattering angles from 5^o to 130^o. These measurements are made to monitor the role of the $^2B_{2g}$ (≈1.8 eV) and the higher $^2B_{2u} + {}^2B_{1u} + {}^2A_g$ (≈7.5 eV) resonances in the scattering dynamics. Our differential cross section measurements are in very good to excellent agreement with past measurements, and in reasonable agreement with theory as regards forward scattering. A feature in the elastic cross section at 90^o scattering angle at ≈ 3.5eV is tentatively associated with the onset of excitation of the $\tilde{a}^3B_{1u}$ triplet electronic state. Differential cross sections for vibrational excitation of four composite energy features in ethylene are also presented from incident energies of 1.25 eV to 15 eV. These results are compared to previous measurements with satisfactory results regarding resonant behavior of these features also concerning the role of the $^2B_{2g}$ (≈1.8 eV) and the higher $^2B_{2u} + {}^2B_{1u} + {}^2A_g$ (≈7.5 eV) resonances in the scattering dynamics.

PACS number(s): 34.80.Bm, 34.80.Gs

email: *mkhakoo@fullerton.edu*

1. **Introduction**

Electron interactions with ethylene or ethene (C_2H_4) have been extensively studied, both theoretically and experimentally, especially with regard to resonant elastic scattering and vibrational excitation. Allan *et al.* [1] carefully investigated resonant processes through measurements of both the elastic and inelastic (including vibrational) channels. More recently, ethylene has also been studied theoretically for inelastic processes involving electronic excitation [2,3]. The dynamics of low energy electron attachment to the C=C double bond is of great interest as this gives rise to vibrational resonances. In some molecules this can cause dissociation (dissociative electron attachment, DEA), but not in ethylene, where electronic excitation is more likely to cause dissociation [1,4,5]. Ethylene is the simplest molecule that comprises the C=C bond and thus the simplest to look at resonances associated with this bond. Low energy DEA of ethylene, giving rise to H^- anions, was recently measured by Cadez *et al*. [4] who observed a weak, composite structure of 3 overlapping features at ≈7.5eV, 9eV and 10.7eV. More recently, the more detailed DEA measurements of Szymańska *et al*. [5] confirmed this H^- structure, but in addition were also able to observe C^-, CH^- and CH_2^- anion fragments at 15 eV, 10 & 15eV and 10eV, respectively. They also observed the fragments $C_2H_3^-$, $C_2H_2^-$, C_2H^- and C_2^- at energies of 7.5 eV & 10.5 eV for the first three anions and 10.5 eV for C_2^-. Low-energy electron collisions with ethylene have also been of interest in modeling low temperature plasmas as well as for their role in basic combustion of a primary hydrocarbon.

Electronically elastic scattering coupled to vibrational excitation of ethylene has also been previously studied, focused on resonant scattering involving electron attachment to the C=C and the C-H_2 bond systems. Elastic scattering measurements were made by Mapstone and Newell [6], Panajotovic *et al*. [8], Khakoo *et al*. [9] and by Allan *et al*. [1]. The first of such resonance measurements were made at high resolution by Walker *et al*. [7] which dealt with vibrational

excitation. Importantly the work of Allan *et al*. [1], also with high resolution, extended the study of [7] to observe the roles of resonances in both elastic and inelastic (vibrational excitation and electronic excitation to the $\tilde{a}^3B_{1u}$ triplet electronic state) processes and the effect of polarization in the excitation of the $\tilde{a}^3B_{1u}$ electronic state. The studies of Allan *et al*. [1] and Panajotovic *et al*. [8] investigated the role of the π^* resonance in the elastic channel. Additional studies of vibrational excitation in ethylene were made by Lunt *et al*. [10] and Mapstone *et al*. [11]. Walker *et al*. [7] concluded that low energy vibrational excitation of C_2H_4 was dominated by shape resonances of π^* $^2B_{2g}$ (≈1.8eV) symmetry, accommodating the incident electron in the first unoccupied $1b_{2g}(\pi^*)$ orbital, and σ^* ^2A_g (≈7.5eV), accommodating the incident electron in the next higher $4a_g(\sigma^*)$ orbital. Importantly, Allan *et al*. [1] confirmed their high resolution work for the π^* $^2B_{2g}$ resonance at 1.8 eV, although they did not provide an assignment for the higher 7.5 eV resonance. Total cross section (TCS) measurements were taken by Floeder *et al* [12], Sueoka and Mori [13], and Lunt *et al*. [10] at collision energies E_0 between 1 eV and 400 eV. Szmytkowski *et al*. [14] have also investigated the effect of shape resonances on the TCS. In particular, Lunt *et al*. [10] used a high resolution (5 meV) photoemission source of electrons, varying E_0 from 0.2 eV to 11 eV and focusing on structure associated with the $^2B_{2g}$ resonance, which they placed at E_0≈2eV. Recently, electronic excitation of ethylene was considered by Do *et al.* [15], who measured the DCSs for the $\tilde{a}^3B_{1u}$ triplet electronic state at similar E_0 as [1] plus at E_0 = 30eV and 50eV. They found very good agreement with the DCSs of [1].

Some of the theoretical studies involving elastic scattering from ethylene include the complex Kohn (CK) variational calculations of Schneider *et al.* [16], the Schwinger variational iterative method (SVIM) calculations of Brescansin *et al*. [17] and the Schwinger multichannel method (SMC) [18] calculations of Winstead et al. [19]. We also note the vibrationally-averaged complex Kohn (VCK) calculations of Trevisan *et al*. [20, 21], who calculated elastic cross

section for ethylene over a range of different geometries, obtaining cross sections both including and excluding the effects of nuclear motion. Theoretical modeling for electron impact excitation of the $\tilde{a}^3B_{1u}$ triplet electronic state has been carried out using the SMC method by Allan *et al.* [1] and using the multi-channel Schwinger method with pseudopotentials (SMCPP) by da Costa *et al.* [2], followed by similar work [3] looking more closely at the convergence of the calculations for elastic scattering and excitation of the $\tilde{a}^3B_{1u}$ state as a function of the number of excited states included, at higher E_0 values, comparing their calculations with the experiments of [1] and [15]. Agreement between the calculations and experiments was good.

In this work, we present DCS measurements for ethylene over a range of E_0 from 0.5 eV to 100 eV and scattering angles (θ) from 5^o to 130^o, with finer E_0 intervals around the $^2B_{2g}$ resonance. Our elastic scattering results are compared to above-mentioned measurements and calculations of the elastic DCSs as well as the total cross sections. We also present vibrational excitation cross sections for 4 features for E_0 ranging from 1.25 eV to 15 eV, to compare with the existing results of Walker *et al*. [7], Allan *et al*. [1] and Mapstone *et al*. [11]. We note that our energy resolution is significantly lower energy than in Refs. [7] and [1], which restricts our work to groups of vibrational energy loss features. We integrated our DCSs to obtain elastic integral cross sections (ICS) and elastic momentum transfer cross sections (MTCS) and compare our results to available total cross section measurements [13,14] and to theory [19].

2.1. Experimental

Our experimental apparatus has been well tested and extensively detailed in previous papers, e.g. Khakoo *et al*. [22], and only a summary of it is given here. The apparatus consisted of a monoenergetic electron gun, aperture-geometry gas source and scattered electron detector, housed in a high vacuum chamber. Both the electron gun and detector were constructed from

titanium and employed cylindrical geometry transport lenses with double hemispherical energy selectors. The system was baked to about 130^{o} using magnetically free biaxial heaters [23] to aid the long term stability of the system. Electrons were detected by a discrete dynode electron multiplier with a background rate of <0.01Hz and capable of linearly detecting $>10^{5}$ Hz without saturating [24]. Typical electron currents were around 15-25 nA, with a total system energy resolution of between 38-50 meV, full-width at half-maximum. Lower currents were chosen for lower E_0 values in order to curtail the effects of space charge broadening of the incident electron beam (so that we could measure scattering at lower θ values without the problems associated with detecting the primary electron beam), and also for vibrational excitation so as to simplify unfolding the vibrational excitation energy loss spectrum by allowing for higher energy resolutions, thus better resolving adjacent features. The electron beam could be easily focused at 1eV and remained stable, varying less than 10% at maximum during the day's data taking. The energy of the beam was regularly established by measuring the dip in the elastic scattering caused by the $2^{2}S$ He^{-} resonance at 19.366 eV [25] at $\theta = 90^{o}$ to better than ≈50meV stability during an experimental run (1 day). Energy loss spectra of the elastic peak were collected at fixed E_0 values and θ by repetitive, multi-channel-scaling techniques.

The target gas beam was formed by the effusive flow of gas through a 0.3mm diameter aperture, which was amorphous carbon-coated (sooted, using an acetylene flame) to reduce secondary electron emission. In using the aperture instead of a conventional tube gas collimator, we obviate the experimental need to maintain the gas pressures of the target gases in an inverse ratio of their molecular diameters, thus removing a systematic source of error that could occur in using tube collimators or similar [9]. The aperture, located about 8 mm below the axis of the electron beam, was incorporated into a moveable source arrangement [26] which is able to determine background spectra accurately and quickly without having to switch gases from the source tube

into a background side tube. This moveable source arrangement is important when low energy electron scattering rates are to be accurately determined especially in the forward scattering θ region, as background scattering can be significant (> 20%) at small scattering angles. The measured DCSs were normalized using the Relative Flow Method with helium as the reference gas, using DCSs from the well-established work of Nesbet [27] for E_0 below 20eV and of Register *et al*. [28] and Boesten and Tanaka [29] for E_0 above 20eV. Ethylene gas used was 99.7% pure, with predominantly hydrocarbon impurities. The source operating pressures behind the aperture ranged from 1.2 to 2 torr for He and 0.12 torr to 0.25 torr for ethylene, resulting in a chamber pressure ranging from $1.2x10^{-6}$ torr to $2x10^{-6}$ torr. Each set of DCSs at a given E_0 value was taken a minimum of two times to check its reproducibility. A weighted average was made of multiple data sets to obtain the final DCSs. These DCSs are given along with 1 standard deviation error bars in Table 1. The errors include the uncertainty in the elastic DCSs for helium (5% - 7%), counting statistics (<1%), uncertainties in the measured gas flow rates (2% per gas) and differences in reproducibility (2%).

For the vibrational excitation experiment, electron energy loss spectra on the energy loss range of -0.15 to 0.65 eV were taken at 1.25, 1.5, 1.75, 2, 3, 4, 5, 8 and 15 eV for the same angles as the elastic scattering data. A sample spectrum is given in Figure 1. These spectra were unfolded using the energies of vibrational modes given in Table 2 obtained from NIST [30] which are similar to those used in [7,1]. In this case each spectrum was taken twice and in some cases up to four times to check reproducibility of unfolded intensities. The DCSs for vibrational excitation were obtained by normalizing, to the elastic DCS of this work, the intensity ratios of the vibrational features to the elastic feature taken in the same energy loss spectrum. In the unfolding algorithm, because of our restricted energy resolution of 38-45meV, it was necessary to group energy loss features as shown in Table 1, to obtain reproducible DCSs with reasonable

statistics. This reduces the detail that could be obtained on the excitation of individual vibrations, compared with the higher resolution data of Walker *et al*. [7] (resolution 22 meV) and Allan *et al*. [1] (20 meV). Nevertheless, our results complement these earlier works and shed further light on the scattering dynamics.

3. Results and Discussion.

3.1 Elastic Scattering.

Our experimental DCSs for elastic electron scattering from ethylene are listed in Table 2. As described above, these DCSs were used to determine the elastic ICS and MTCS, which are also listed in Table 2. The present elastic DCSs are in very good agreement (within error bars in most cases) with previous measurements from our group taken by Khakoo *et al*. [9]. The DCSs of Khakoo et al. [9] were taken over a much smaller range of E_0 values, 2 eV, 5 eV, 10 eV, 20 eV and 30 eV, at a maximum of 9 scattering angles ranging from 10^o to 130^o. The measurements of [9] were primarily made simply to test the efficacy of Relative Flow Method when using an aperture gas source. The present measurements are taken at significantly more E_0 values and over more values of θ. Consequently, these earlier DCSs of [9] are not included in comparisons here and the present work is considered to supersede them.

The present elastic DCSs were also taken at more closely spaced E_0 values around the region of 1.25 eV to 2.5 eV, i.e., where the $\pi^*\ ^2B_{2g}$ resonance is. Figures 2a show the trend of the angular distribution for E_0 from 0.5 eV to 2.5 eV. At E_0 = 0.5 eV the scattering shows basic polarization potential scattering, i.e. a forward-peak merging into a backward peak without any mid-angle structure, the former due to long-range scattering via the (significant) polarizability of ethylene of 4.17 a_0^3 (Cooper *et al*., 31). At higher energies, we see in Figures 2a that the dπ distribution due to $\pi^*\ ^2B_{2g}$ resonance sets in around E_0 = 1eV and persists until 3eV. This range

of E_0 from 1eV to 3eV was also observed by [1,7], except here our results track it in the elastic scattering channel only whereas [1] tracks it in both elastic and vibrational excitation channels and [7] only in the vibrational excitation channels. The energy of the resonance peak was established by Allan *et al*. to be around E_0 = 1.8 eV, whereas Szmytkowski *et al*. (2003) find it in their total cross section measurements (TCS) to be somewhat higher at E_0 = 1.9eV (see also later), although the energy resolution of Allan *et al*. is higher and thus presumably more accurate. The work of Walker *et al*. [7] shows this resonance to be quite broad with a width of about 0.7 eV, significantly affecting essentially all symmetries of vibrational modes. We will comment on this later. The present elastic DCSs at 1.5 and 5eV (Figures 2) show excellent agreement with Allan *et al*. [1] at both E_0 values where they have published their DCSs, and they are in good agreement with the results of Panajotovic *et al*. [8] at large θ, but at small θ the data of Ref. [8] do not display the forward scattering observed in the present work and in Ref. [1] below 5eV . We have also included the DCSs of [1] from their excitation functions at θ=10^o, 45^o, 90^o, 135^o and 180^o and observe excellent agreement with all their DCSs. We have checked our spectrometer's response regarding the forward scattering at energies below 1.5eV and small θ, with the DCSs for elastic scattering from N_2 [33] and [35, p. 283] which is isoelectronic with C_2H_4. Whereas N_2 DCSs do not show any forward scattering, forward scattering in C_2H_4 persists even at E_0 = 0.5eV. At 1.0eV, the SMC and SVIM theory show clear forward scattering, but not as pronounced as our measurements. At these low energies, the VCK result [16] (which includes nuclear dynamics) and CK results [21] surprisingly display more of a backward scattering distribution and show a significantly less forward scattering than observed in the experiment. In fact, at most angles forward scattering is more pronounced in the present measurements than in any theoretical DCS, of which the SMC results [19] give best agreement with experiment in terms of forward peaking. The rapidly changing angular distributions at low E_0 values below 5

eV is typical of electron scattering from aliphatic hydrocarbons and has been seen in many experiments.

At E_0 values above 5eV, agreement with theory typically improves, with best agreement around 8 to 15eV. Above 15eV, the neglect of ionization and other significant open channels makes electron-polyatomic elastic scattering models of the SMC type less accurate and gives rise to disagreement between theory and experiment. At higher E_0, agreement of the present experiment with those of Panajotovic *et al*. [8] and of Mapstone and Newell [5] is very good to excellent. Both elastic scattering experiment and theory show some backward scattering. Good agreement is also observed with the most recent SMCPP theory [3].

The effect of the dominant π^* $^2B_{2g}$ resonance is observed in Figure 3 where elastic scattering at $\theta=90^o$ is measured as a function of E_0. Our measurements (see Figure 3) show this maximum to be at 1.7 eV in good agreement with Allan *et al*. [1] (1.8 eV) and with Szmytkowski *et al*. [14] (1.9 eV). This shape resonance (as will be later discussed) also affects the vibrational excitation of C_2H_4 producing boomerang structures in the excitation cross sections of the C=C stretch mode and its overtones (up to 4x), as was observed weakly at first by Walker *et al*. [7] and more clearly by Allan *et al*. (2008). We also see a distinct raised feature that extends from E_0 = 3.0eV to 5.2eV. This coincides energetically with the excitation energy of the $\tilde{a}^3B_{1u}$ triplet electronic state which extends in the Franck-Condon region of 3.2eV to 5.9eV as observed by Allan *et al*. [1], and could possibly suggest the decay of a near-threshold core-excited resonance into the elastic channel. This feature is not clearly observed in the excitation functions of either Panajotovic *et al*. [8], Allan *et al*. [1] or Lunt *et al*. [10]. Lunt *et al*. may be excluded here as these are TCSs, summed over all θ. The feature is, however, observed in the DCSs (at $\theta = 90^o$) of the Sophia University DCS data in Panajotovic *et al*. [8] as well as in our $\theta = 90^o$ DCS measurements, these DCSs all having been taken independently of the excitation curves.

The elastic scattering DCSs were integrated in the standard way as described in a previous paper [32]. Figures 4a, b show the present ICSs and MTCSs for elastic scattering compared to the experiment of [8] and the TCS measurements of [13,14] as well as the SMC theory [8,9,33]. Agreement between all these data is good in general although the TCSs of [13] are lower than our ICSs in the $^2B_{2g}$ π resonance region for E_0 from 1.5 to 2.5 eV. The TCSs of [14] are higher by about 10-15% below E_0=10 eV, and this is because they include inelastic (mainly vibrational excitation) scattering. Above the ionization potential of ethylene at 10.514 eV [34], with the opening of ionization pathways, this difference increases to 30% and is about 130% at the largest E_0 of 100eV. Agreement of our MTCS with other experimental and theoretical values is very good. The SMC theory displays a significantly sharper $^2B_{2g}$ resonance at $E_0 \approx 2$ eV because of the neglect of vibrational motion in the calculation, but it is otherwise in very good quantitative agreement with experiments overall.

3.2. Vibrational Excitation.

Our vibrational excitation DCSs were taken at E_0 values of 1.25 to 15 eV and for θ from 15^o to 130^o. Since they form a very large data set, we have not tabulated them here, but they are available from the main author on request. These DCSs were also integrated as in described in Ref. [32] to obtain integral cross sections (ICS), which are also available on request.

Figure 5 shows E_0=8 eV and 15 eV DCSs for the sum of the first two features (equivalent to v_i in Mapstone *et al*., Ref. [11]) and the last feature (v_j in [11]). Agreement is good in most cases including the angular distributions. Error bars range in the above 20% levels at 5 eV and above 25% levels at 8 eV. The distributions are nominally flat, showing the major influence of the ^2A_g shape resonance according to the assignment of [7] in the region around E_0=7.5 eV, which has a width of ≈ 5eV as shown in Figure 6 for the 0.379 eV excitation function (width is given as ≈ 4

eV in [7]). However, a molecular orbital calculation using a minimal basis set [33] suggests the 7.5 eV peak results from overlapping CH σ* resonances of $^2B_{2u}$, $^2B_{1u}$ and ^2A_g symmetries, which supports the association between this feature and excitation of the CH modes listed in feature 4, Table 2. However, we can no longer explain the isotropic distribution on the grounds of the peak being due to a single resonance of ^2A_g symmetry as was done in Ref. [7]. Figure 6 also shows "excitation functions" for other pertinent energy losses to compare with [7,1]. These are obtained by fixing the energy loss at the given value on the spectrometer and monitoring the scattered counts at the fixed $\theta = 90^o$ as a function of E_0. These relative counts are normalized to our elastic DCSs for features 1 to 4 respectively at the resonance peak around E_0=2 eV. Apart from feature 4, our results are higher at above 3 eV than those of Ref. [7] because of our broader resolution which includes excitations outside of the nominal energy loss for exciting a single vibrational mode at the energy loss setting. Nevertheless, we can mostly observe as afore-known that all modes are affected by the longer lived $^2B_{2g}$ and relatively shorter lived 7.5eV shape resonances across their E_0 ranges. Feature 4, which is a sum over several C-H stretch modes (see Table 2), is excited significantly more in the 7.5 eV energy range. In Figure 7, we show DCSs for the four features. For the first feature, the d-wave distribution due to the π* $^2B_{2g}$ resonance at 2eV does not affect this feature as strongly as it does the others (especially feature 3), but it nevertheless excites these modes. Feature 2, 3 and 4 are all enhanced by resonant scattering, especially the C=C excitation at low E_0 values, as has been well-established before. In fact the DCS for feature 3 (the C-C stretch) is increased in size by a factor of 2 at E_0=1.75 eV or 2 eV when comparing to E_0=8eV which is the next highest in magnitude. This mode shows a persistent d-wave angular distribution even at E_0=5eV. Finally the ICSs for features 1-4 are shown in Figure 8 and show clear enhancement of the cross sections in the region of the sharper and longer-lived $^2B_{2g}$ shape resonance and shorter-lived and broader energy width ^2A_g shape resonance. These cross sections

are much smaller at around E_0=3 to 5eV, i.e. in between the region of the $^2B_{2g}$ and the $^2B_{2u}$, $^2B_{1u}$ and ^2A_g shape resonances. Enhancement of the C=C stretch vibration at 0.201 eV energy loss is the most prevalent of all the modes pumped by the $^2B_{2g}$ resonance, as has been shown before by [7,1].

4. Conclusions.

The present work has presented DCSs for elastic scattering from C_2H_4 over a large range of energies from 0.5 eV to 100 eV. Our results are in very good agreement with previously measured DCSs, especially those of Allan *et al.* [1] where agreement is excellent. The cross section displays clear forward scattering at low energies, clarifying the low energy elastic DCS picture for theoretical models to reproduce. Forward scattering, and in some cases backward scattering, in the elastic channel at low energies is not completely accounted for by theory, possibly indicating the need for larger calculations that better address polarization and/or long-range (or equivalently high partial-wave) scattering. An interesting feature in our 90^o scattering elastic excitation function coincides in energy with the excitation energy of the a^3B_{1u} triplet electronic state which extends in the excitation Franck-Condon region of 3.2 eV to 5.9 eV as observed by Allan *et al*. [1], and we tentatively assign this to a threshold coupling between elastic and electronic excitation channels. Further, independent, work to confirm this assignment would be desirable. Our lower resolution vibrational excitation DCSs also provide angular distributions and magnitudes for groups of vibrational excitations that point to enhancement via C-C π^* ($^2B_{2g}$) and C-H σ^* ($^2B_{2u}$, $^2B_{1u}$, and ^2A_g) shape resonances, showing regions of dπ and sσ angular distributions, respectively, and complement the work of Walker *et al*. [7] and Allan *et al*. [1]. However, theoretical work on the vibrational excitation of the C-H and C=C modes of ethylene is needed to fully understand the observed resonant behavior.

5. Acknowledgements.

This work was funded by the National Science Foundation research grants NSF-RUI-AMO 1306742 and 0968874. Important discussions with, and supporting data from, Carl Winstead on this work (especially concerning the symmetry and role of shape resonances) are very gratefully acknowledged. We also thank Carl Winstead and Vince McKoy for providing tabulations of their elastic scattering Schwinger Multi-Channel calculations, Cynthia Trevisan and Ann Orel for providing tabulations of their variational complex Kohn (VCK) calculations and Romarly F. da Costa for sending us tabulations of their Schwinger Multi-channel with pseudopotentials (SMCPP) results. High school students Justin Lee and Ryan Murase worked under a Troy Tech High School summer internship program in our laboratory.

6. References.

[1] M. Allan, C. Winstead and V. McKoy, Phys. Rev. A **77**, 042715 (2008).

[2] R. F. da Costa, Márcio H. F. Bettega, and M. A. P. Lima, Phys. Rev. A **77**, 042723 (2008).

[3] R. F. da Costa, M. H. F. Bettega, M. T. do Varella, E. M. de Oliveira and M. A. P. Lima, Phys. Rev. A **90**, 052707 (2014).

[4] I. Cadez, S. Markejl and Z. Rupnik, Eur. Phys. J. D **66**, 73 (2012).

[5] E. Szymańska, N. J. Mason, E. Krishnakumar, C Matias, A. Mauracher, P. Schier and S. Denifl, Int. J. Mass Spectry. **365 - 366**, 356 (2014).

[6] B. Mapstone and W. R. Newell, J. Phys. B: At. Mol. Phys. **25**, 491 (1992).

[7] I. C. Walker, A. Stamatovic and S. F. Wong, J. Chem. Phys. **69**, 5532, (1978).

[8] R. Panajotovic, M. Kitajima, H. Tanaka, M. Jelislavcic, J. Lower, L. Campbell, M. J. Brunger and S. J. Buckman, J. Phys. B: At. Mol. Phys. **36**, 1615 (2003).

[9] M. A. Khakoo, K. Keane, C. Campbell, N. Guzman and K. Hazlett, J. Phys. B: At. Mol. Phys. **40**, 3601 (2007).

[1] M. Allan, C. Winstead and V. McKoy, Phys. Rev. A **77**, 042715 (2008).

[10] S. L. Lunt, J. Randell, J. P. Ziesel, G. Mrotzek and D. Field, J. Phys. B: At. Mol. Phys. **27**, 1407 (1994).

[11] B. Mapstone, M. J. Brunger and W. R. Newell, J. Phys. B: At. Mol. Phys. **33**, 23 (2000).

[12] K. Floeder, D. Fromme, W. Raith, A. Schwab and G. Sinapius, J. Phys. B: At. Mol. Phys. **18**, 3347 (1985).

[13] O. Sueoka and S. Mori, J. Phys. B: At. Mol. Phys. **19**, 4035 (1986).

[14] C. Szymytkowski, S. Kwitnewski and E. Ptasińska-Denga, Phys. Rev. A **68**, 032715 (2003).

[15] T. P. T. Do, K. L. Nixon, M. Fuss, G. Garcia, F. Blanco and M. J. Brunger, J. Chem. Phys. **136**, 184313 (2012).

[16] B. I. Schneider, T. N. Rescigno, B. H. Lengsfield and C. W. McCurdy, Phys. Rev. Letts. **66**, 2728 (1991).

[17] L. M. Brescansin, L. E. Machado and M-T. Lee, Phys. Rev. A **57**, 3504 (1998).

[18] C. Winstead, P. G. Hipes, M. A. P. Lima and V. McKoy, J. Chem. Phys. **94**, 5455 (1991).

[19] C. Winstead, V. McKoy, and M. H. F. Bettega, Phys. Rev. A **72**, 042721 (2005).

[20] C. S. Trevisan, A. E. Orel and T. N. Rescigno, Phys. Rev. A **68**, 062707 (2003) and

[21] C. S. Trevisan, Private Communication (2015).

[22] M. A. Khakoo, C. E. Beckmann, S. Trajmar and G. Csanak, M. A. Khakoo, C. E. Beckmann, J. Phys. B **27**, 3159 (1994).

[23] ARi Industries Inc., Addison, IL 60101 USA, 1HN040B-16.3 biaxial cable.

[24] ETP Equipe Thermodynamique et Plasmas (ETP) model AF151.

[25] J. H. Brunt, G. C. King, and F. H. Read, J. Phys. B: At. Mol. Phys. **10**, 1289 (1977).

[26] M. Hughes, K. E. James, Jr., J. G. Childers, and M. A. Khakoo, Meas. Sci. Technol. **14**, 841 (1994).

[27] R. K. Nesbet, Phys. Rev. A **20**, 58 (1979).

[28] D. F. Register, S.Trajmar, and S. K. Srivastava, Phys. Rev. A **21**, 1134 (1980).

[29] L. Boesten and H. Tanaka, At. Data Nucl. Data Tables, **52**, 25 (1992).

[30] T. Shimanouchi, Tables of Molecular Vibrational Frequencies Consolidated Volume I, National Bureau of Standards, 1 (1972).

[31] G. Cooper, T. N. Olney and C. E. Brion, Chem. Phys. **194,** 175 (1995).

[32] K. Fedus, C. Navarro, L. R. Hargreaves, M. A. Khakoo, F. M. Silva M. H. F. Bettega, C. Winstead and V. McKoy, Phys. Rev. A **90**, 032708 (2014).

[33] C. Winstead, Private Communication, 2015.

[34] B. A. Williams and T. A. Cool, J. Am. Chem. Soc. **94** 6358 (1991).

[35] M. J. Brunger and S. J. Buckman, Phys. Rep. **357**, 215 (2002).

6. Tables.

Energy (eV)→	DCS (10^{-16}cm^2/sr)																			
Angle (^{o})↓	0.50	Error	0.75	Error	1.00	Error	1.25	Error	1.50	Error	1.75	Error	2.00	Error	2.50	Error	3.00	Error	4.00	Error
0	*1*		*1.4*		*3.8*		*3.3*		*6.2*		*8*		*6*		*5*		*4*		*7*	
5	*0.85*		*1.3*		*3.3*		*2.9*		*5.4*		*6.8*		*5.4*		*4.5*		*3.5*		*6*	
10	*0.7*		*1.2*		*2.8*		*2.6*		*4.7*		*5.8*		*4.7*		*3.9*		*3*		5.02	0.61
15	*0.65*		*1.05*		*2.4*		*2.2*		*3.96*		*4.8*		*4.2*		*3.4*		2.64	0.32	3.84	0.42
20	*0.55*		*0.95*		1.78	0.30	2.02	0.24	3.26	0.44	4.15	0.55	3.79	0.49	3.12	0.39	2.26	0.28	3.33	0.38
25	0.488	0.103	0.81	0.14	1.27	0.15	1.69	0.20	2.28	0.25	3.42	0.43	3.29	0.37	2.68	0.34	2.00	0.21	2.82	0.34
30	0.439	0.076	0.636	0.112	0.936	0.111	1.29	0.15	1.98	0.22	2.68	0.33	2.90	0.32	2.34	0.29	1.89	0.20	2.48	0.30
35	*0.409*		*0.552*		*0.779*		*1.03*		*1.61*		2.30	0.28	*2.64*		*2.27*		*1.84*		*2.46*	
40	0.380	0.056	0.428	0.057	0.622	0.074	0.765	0.085	1.24	0.14	2.00	0.24	2.39	0.26	2.19	0.27	1.80	0.20	2.44	0.30
50	0.357	0.051	0.383	0.049	0.636	0.072	0.871	0.101	1.16	0.14	1.59	0.20	2.11	0.23	2.05	0.26	1.91	0.21	2.42	0.29
60	0.320	0.046	0.401	0.050	0.767	0.092	1.14	0.12	1.43	0.17	1.60	0.19	2.09	0.22	1.90	0.25	1.82	0.21	2.17	0.25
70	0.381	0.053	0.485	0.065	1.14	0.128	1.46	0.16	1.89	0.22	1.94	0.22	2.24	0.25	1.97	0.24	1.63	0.19	2.04	0.21
80	0.405	0.056	0.661	0.088	1.28	0.140	1.70	0.20	2.15	0.25	2.16	0.26	2.19	0.25	1.89	0.24	1.48	0.16	1.70	0.19
90	0.494	0.068	0.727	0.090	1.44	0.163	1.93	0.20	2.31	0.24	2.21	0.28	2.15	0.25	1.69	0.22	1.22	0.13	1.36	0.16
100	0.570	0.074	0.873	0.114	1.43	0.172	1.91	0.21	2.21	0.26	2.05	0.25	1.91	0.20	1.59	0.20	1.08	0.13	1.17	0.14
110	0.614	0.083	1.07	0.12	1.34	0.173	1.68	0.21	1.87	0.20	1.76	0.20	1.71	0.18	1.31	0.17	0.982	0.116	1.13	0.13
120	0.715	0.118	1.15	0.15	1.42	0.156	1.52	0.16	1.63	0.19	1.49	0.18	1.68	0.19	1.27	0.16	0.879	0.105	1.12	0.13
125	*0.8*		*1.2*		1.25	0.136	1.31	0.14	1.40	0.15	1.37	0.17	1.7	0.25	1.25	0.16	*0.898*		1.15	0.13
130	*0.85*		*1.23*		*1*		*1*		*1*		1.56	0.19	1.75	0.25	1.37	0.17	0.917	0.105	1.22	0.14
140	*0.95*		*1.25*		*0.85*		*0.85*		*0.85*		*1.8*		*1.9*		*1.5*		*0.95*		*1.4*	
150	*1.05*		*1.25*		*0.75*		*0.75*		*0.95*		*2.2*		*2*		*1.6*		*1.1*		*1.5*	
160	*1.1*		*1.25*		*0.7*		*0.7*		*1.1*		*2.5*		*2.2*		*1.7*		*1.3*		*1.6*	
170	*1.15*		*1.2*		*0.78*		*0.78*		*1.2*		*2.7*		*2.3*		*1.85*		*1.4*		*1.75*	
180	*1.17*		*1.15*		*0.9*		*0.9*		*1.4*		*3*		*2.5*		*2*		*1.5*		*2*	
ICS	7.4	1.0	10.4	1.6	14.2	1.9	17.3	2.4	21.8	2.9	26.0	3.7	27.1	3.6	22.6	3.0	17.6	2.3	22.2	3.0
MTCS	8.8	1.2	12.3	2.0	14.0	2.5	16.7	2.7	19.6	3.2	24.2	3.8	24.7	3.4	20.0	2.8	14.8	2.0	18.3	2.6

Energy (eV)→	DCS (10^{-16}cm^2/sr)																	
Angle (^{o})↓	5.0	Error	8.0	Error	10.0	Error	15.0	Error	20.0	Error	30.0	Error	40.0	Error	60.0	Error	100.0	Error
0	*9.5*		*19*		*30*		*35*		*60*		*90*		*110*		*130*		*150*	
5	*8*		*17*		*24*		*27*		*40*		*50*		48.0	6.5	47.8	5.9	35.2	4.8
10	*7*		14.6	1.7	16.6	2.1	19.4	2.4	26.5	3.3	27.3	3.4	26.6	2.9	22.1	2.6	15.4	2.1
15	6.11	0.70	12.4	1.4	13.0	1.5	14.9	1.5	17.8	2.1	16.5	1.8	13.7	1.5	10.1	1.2	6.24	0.84
20	4.89	0.56	9.04	1.05	10.4	1.2	11.7	1.3	12.2	1.3	9.85	1.13	7.37	0.78	4.45	0.52	2.52	0.33
25	3.94	0.43	7.50	0.89	7.80	0.90	8.22	0.84	8.55	1.01	5.39	0.58	2.73	0.32	2.23	0.25	1.22	0.16
30	3.34	0.38	5.56	0.60	5.84	0.68	6.35	0.66	4.96	0.51	3.28	0.35	1.66	0.18	1.11	0.12	0.602	0.079
35	*3.07*		*4.54*		*4.72*		*4.60*		*3.54*		*2.31*		*1.19*		*0.806*		*0.447*	
40	2.79	0.29	3.52	0.39	3.60	0.40	2.84	0.33	2.13	0.24	1.33	0.16	0.727	0.074	0.499	0.055	0.293	0.038
50	2.51	0.29	2.39	0.25	2.12	0.21	1.49	0.16	1.13	0.13	0.671	0.075	0.422	0.043	0.308	0.035	0.175	0.025
60	2.34	0.26	1.78	0.20	1.45	0.17	0.997	0.117	0.755	0.080	0.449	0.045	0.244	0.028	0.192	0.022	0.139	0.020
70	1.92	0.21	1.34	0.15	1.10	0.11	0.710	0.078	0.553	0.056	0.314	0.035	0.174	0.018	0.127	0.015	0.093	0.013
80	1.44	0.17	0.99	0.11	0.78	0.09	0.554	0.066	0.449	0.050	0.241	0.026	0.164	0.019	0.116	0.014	0.068	0.009
90	1.13	0.13	0.86	0.09	0.71	0.08	0.525	0.059	0.404	0.041	0.222	0.024	0.149	0.017	0.085	0.010	0.066	0.009
100	1.06	0.12	1.01	0.11	0.97	0.10	0.653	0.071	0.448	0.047	0.256	0.028	0.170	0.019	0.090	0.011	0.068	0.010
110	1.07	0.13	1.45	0.17	1.29	0.15	0.719	0.074	0.514	0.056	0.262	0.029	0.193	0.022	0.114	0.014	0.070	0.010
120	1.20	0.14	1.66	0.19	1.49	0.17	0.796	0.089	0.528	0.060	0.306	0.032	0.235	0.025	0.151	0.019	0.094	0.014
125	1.29	0.14	1.69	0.20	1.48	0.16	0.805	0.091	0.540	0.065	*0.330*		*0.263*		*0.165*		*0.108*	
130	1.33	0.16	1.72	0.20	1.47	0.18	0.804	0.092	0.581	0.067	0.353	0.039	0.291	0.030	0.178	0.023	0.122	0.019
140	*1.5*		*1.8*		*1.7*		*0.85*		*0.65*		*0.45*		*0.4*		*0.27*		*0.18*	
150	*1.7*		*1.9*		*1.8*		*0.9*		*0.75*		*0.6*		*0.55*		*0.35*		*0.27*	
160	*1.8*		*2*		*1.95*		*0.9*		*0.8*		*0.7*		*0.65*		*0.5*		*0.4*	
170	*1.9*		*2.2*		*2*		*0.9*		*0.9*		*0.8*		*0.75*		*0.65*		*0.56*	
180	*2.2*		*2.4*		*2.4*		*0.9*		*0.95*		*0.95*		*0.9*		*0.85*		*0.8*	
ICS	23.8	3.2	28.4	3.7	27.6	3.9	22.7	3.0	21.4	3.0	17.0	2.8	13.2	1.8	10.2	1.4	6.61	0.87
MTCS	18.6	2.7	20.1	2.7	18.2	2.7	10.8	1.4	8.37	1.22	5.48	1.08	4.21	1.01	2.86	0.81	1.61	0.29

Table 1: Present measurements of ethylene elastic electron scattering differential cross sections, integral cross sections and momentum transfer cross sections with error bars (1 standard deviation). Numbers in italics are extrapolated results used to determine ICSs and MTCSs given in the bottom rows. See text for discussion.

Symmetry	Mode	Character	Wave #	ΔE eV			Activity	Feature #	
B_{2u}	ν_{10}	CH_2 rock	826.0	0.1024	±	0.0001	IR	1	a
B_{2g}	ν_7	CH_2 wag	949.3	0.1177	±	0.0001	Raman		b
A_u	ν_4	CH_2 twist	1023.0	0.1268	±	0.0037	Inactive		c
B_{3g}	ν_6	CH_2 rock	1236.0	0.1532	±	0.0007	Raman	2	d
A_g	ν_3	CH_2 scis	1342.2	0.1664	±	0.0004	***Raman***		e
B_{1u}	ν_{12}	CH_2 scis	1443.5	0.1790	±	0.0004	IR		f
A_g	ν_2	CC str	1622.6	0.2012	±	0.0019	***Raman***	3	g
B_{1u}	ν_{11}	CH s-str	2988.7	0.3705	±	0.0001	IR	4	h
A_g	ν_1	CH s-str	3026.4	0.3752	±	0.0004	***Raman***		i
B_{3g}	ν_5	CH a-str	3102.5	0.3847	±	0.0004	Raman		j
B_{2u}	ν_9	CH a-str	3105.5	0.3850	±	0.0004	***IR***		k

Table 2: Vibrational modes of ethylene with symmetries and mode characteristics. Activity column shows the strength of the CH_2 rocking, wagging, scissoring, twisting and the CH symmetric and asymmetric stretch modes. The twist, scissoring and bold-italics indicate strong modes. The energy loss features measured are unfolded composite groupings of modes (last 2 columns). The data is a summary of compilation of Walker *et al*. [7] and Shimanouchi [30]. See text for discussion.

7. Figures.

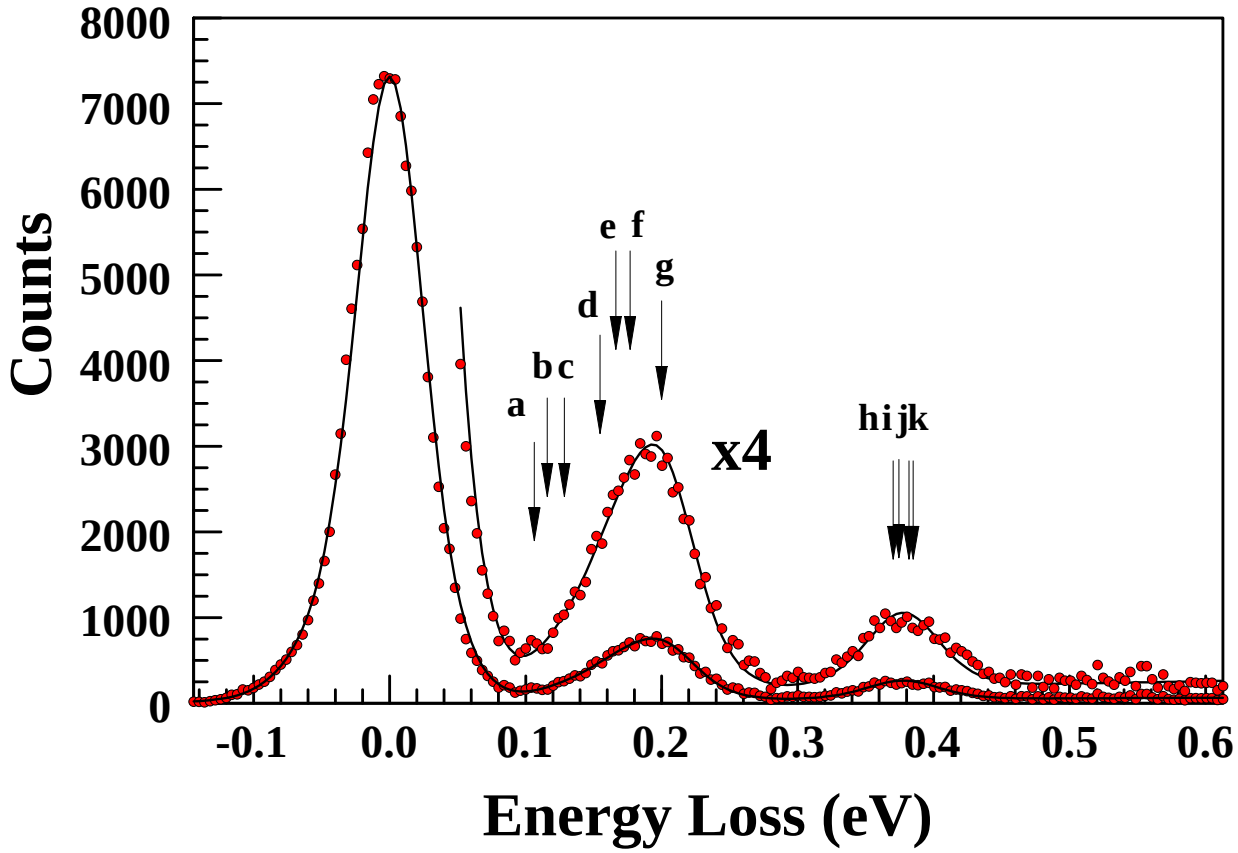

Figure 1 (Color online): Background subtracted electron energy loss spectrum of ethylene at E_0=2 eV and θ=90°. The features arrowed are the same as in Table 1. Black dots are the experimental data and the blue line is the fit to the data.

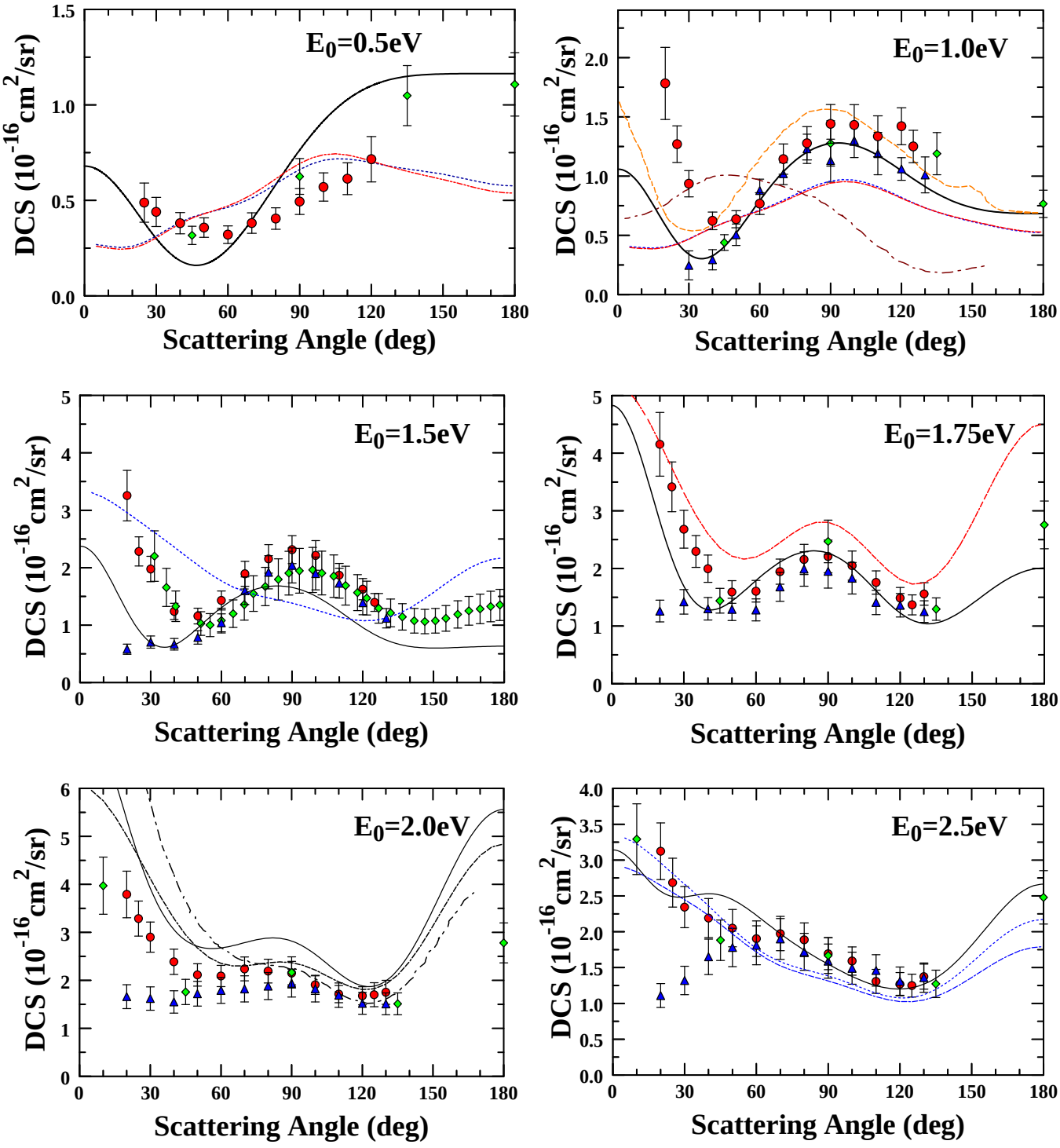

Figure 2a (Color online): DCSs for low energy elastic electron-ethylene scattering. Experiments: ● Present results, ♦ Allan *et al*. [1] digitized from their paper, ▲ Panajotovic *et al*. [8]. Theory: —— Winstead et al., Vibrationally Averaged Multi-Channel Schwinger (Private Comm.), also published in Panajotovic *et al*. [8] and in Khakoo *et al*. [9], — - — Schneider *et al*. [16] Complex Kohn Method also published in [8], --- Trevisan *et al*. [20,21] Complex Kohn Variational Method with adiabatic nuclei, – · – and with fixed nuclei, - - - Brescansin *et al*. [17] Schwinger Variational Iterative Method, also published in [8]. See text for discussion.

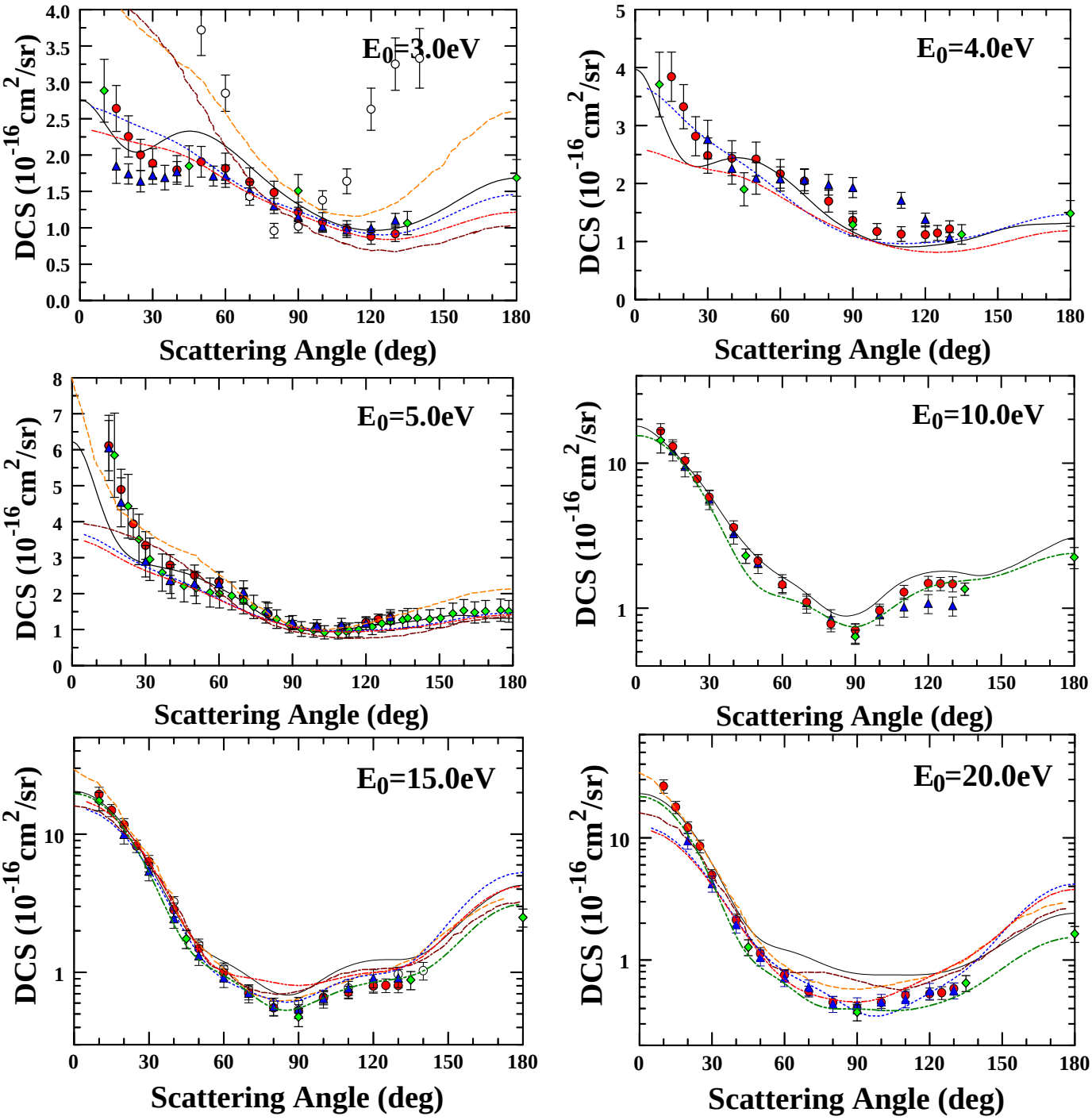

Figure 2b (Color online): DCSs for higher energy elastic electron-ethylene scattering.
Legend: same as 2a except, Experiment: O Mapstone and Newell [6] and Theory: — - - — SMCPP [3]. See text for discussion.

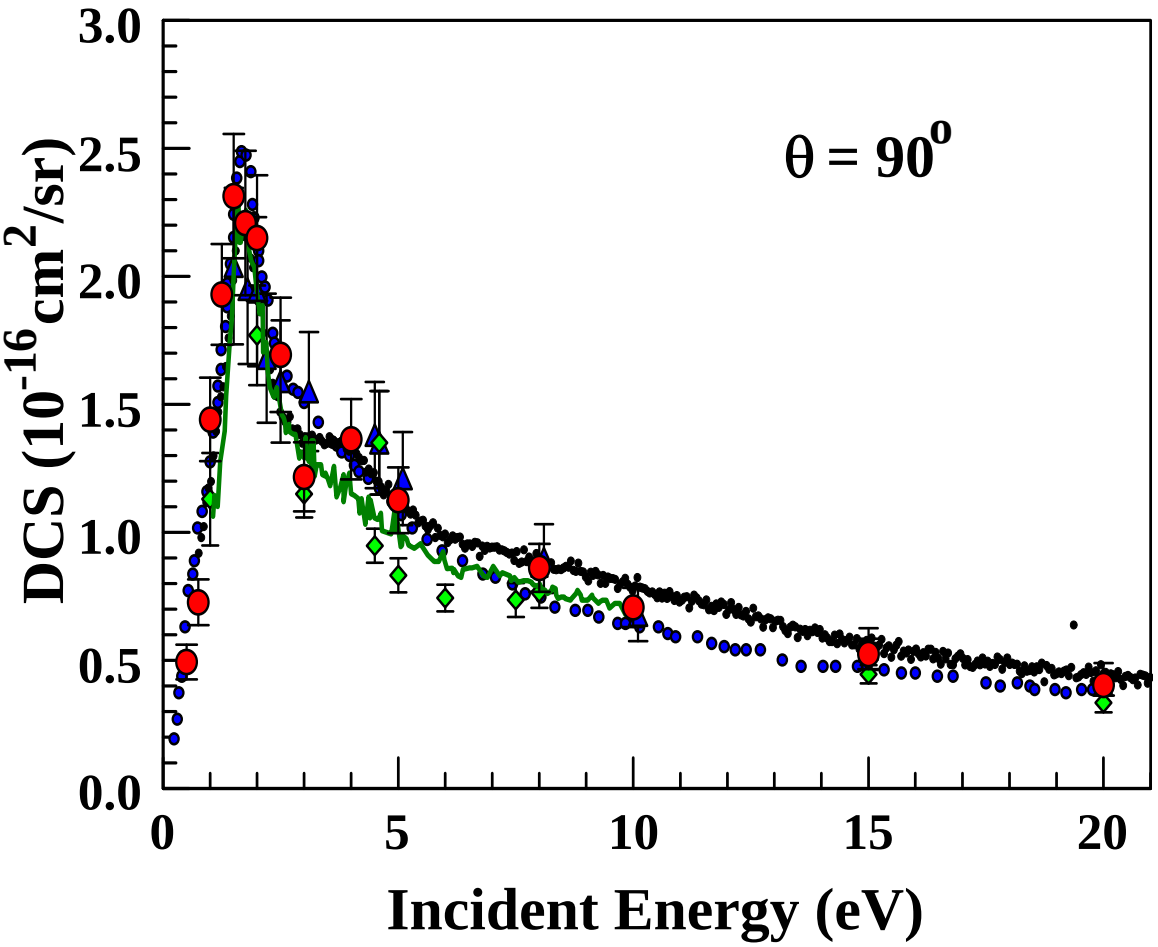

Figure 3 (Color online): Experimental DCSs for elastic electron-ethylene scattering at $\theta=90^{o}$ as a function of E_0. Legend:. ● Present DCS results and present • excitation function, — Panajotovic *et al*. [8] digitized excitation function, ♦ Panaotovic *et al*. [8] ANU DCS data, ▲ Panajotovic *et al*. [8] Sophia U. DCS data. • Allan *et al*. [8] digitized excitation function. See text for discussion.

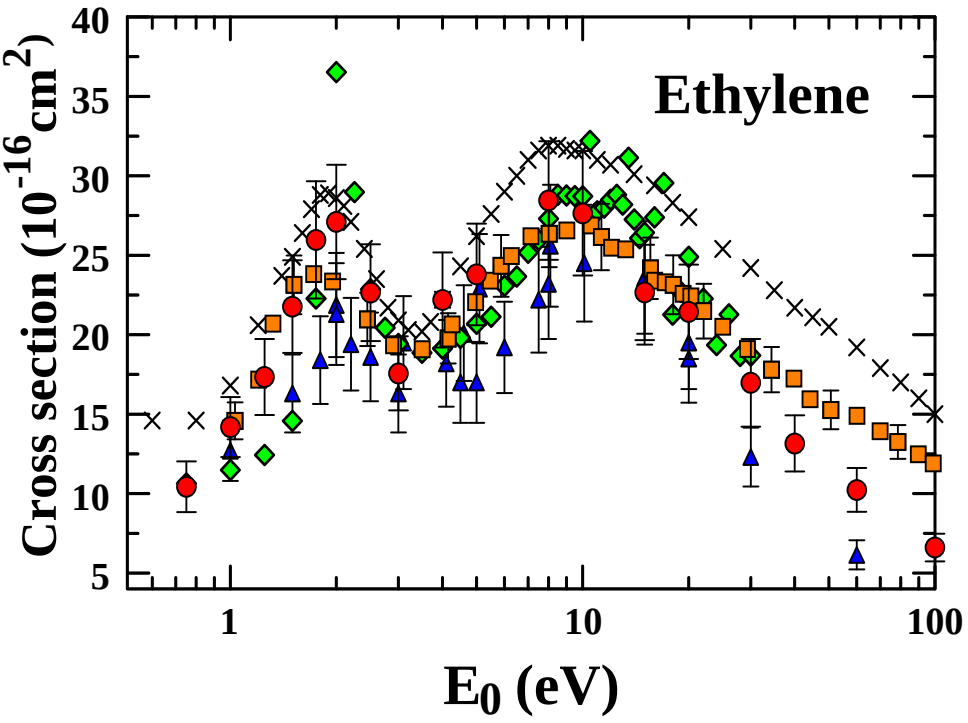

Figure 4a (Color online): Experimental ICSs for elastic electron-ethylene scattering as a function of E_0. Legend: ● Present results, ▲ Panajotovic *et al*. [8], ♦ SMC, Winstead [19]; ■ Sueoka and Mori [13] and × Szmytkowski *et al*. [14] TCSs. See text for discussion.

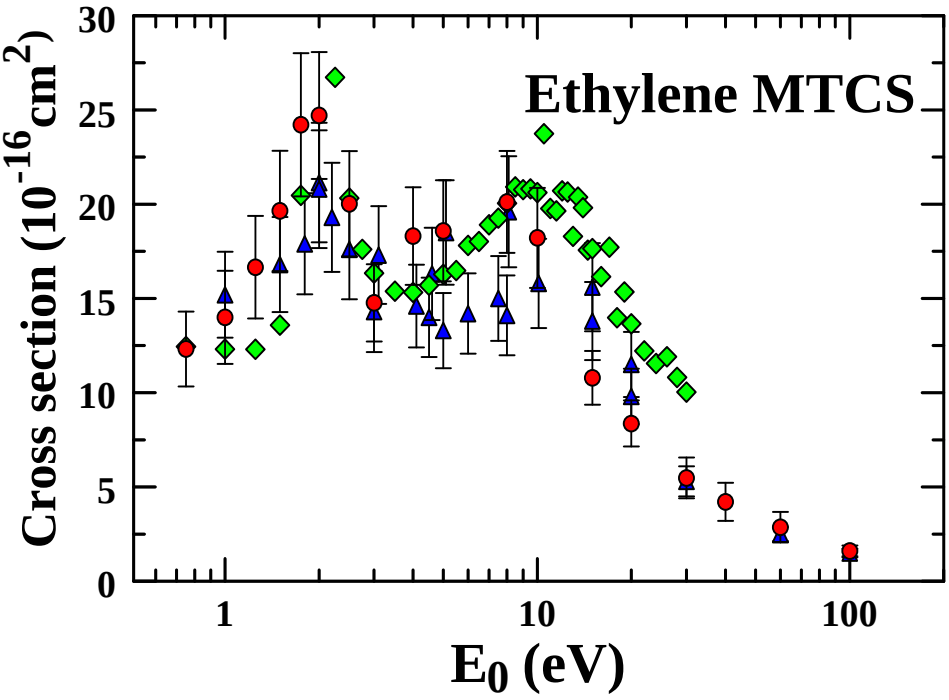

Figure 4b (Color online): Experimental MTCSs for elastic electron-ethylene scattering as a function of E_0. Legend: same as 4a. See text for discussion**.**

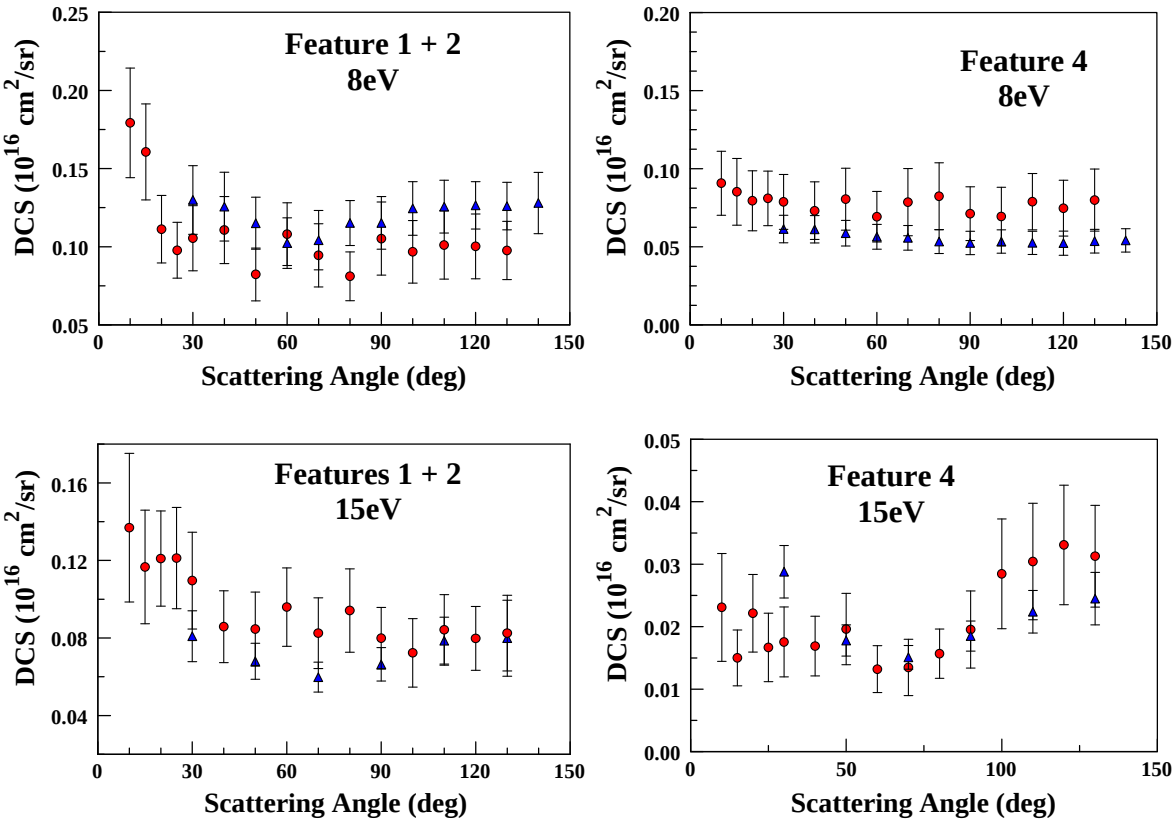

Figure 5 (Color online): Experimental DCSs for vibrational excitation of features in the energy loss summed regions 1 and 2 regions of Table 2 and of region 4 of Table 2 (respectively equivalent to v_i and v_j of Mapstone *et al*. [11]. Legend: ● Present results, ▲ [11].

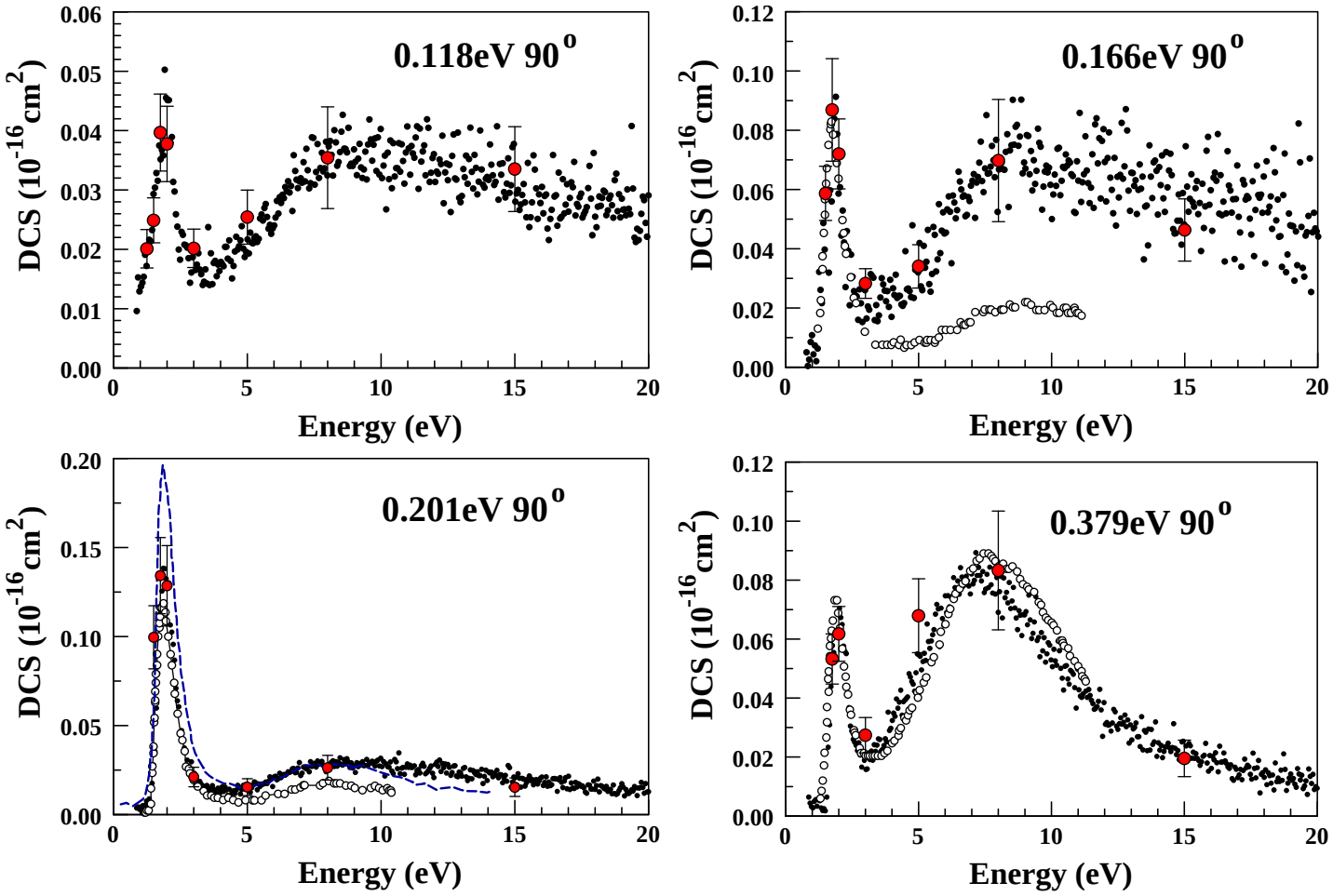

Figure 6 (Color online): Experimental DCSs for vibrational excitation of ethylene for features at the energy loss specified, at the fixed θ of 90°, as a function of energy E_0. Legend: ● Present DCS points at θ=90°, for regions 1, 2, 3 and 4, respectively from Table 1; Excitation functions at the energy losses given in figure: ● Present results normalized to the present regional DCSs, ○ Walker *et al*. [7] digitized data at θ=90°, - - - Allan *et al*. [1] digitized data at θ=180°. See text for discussion.

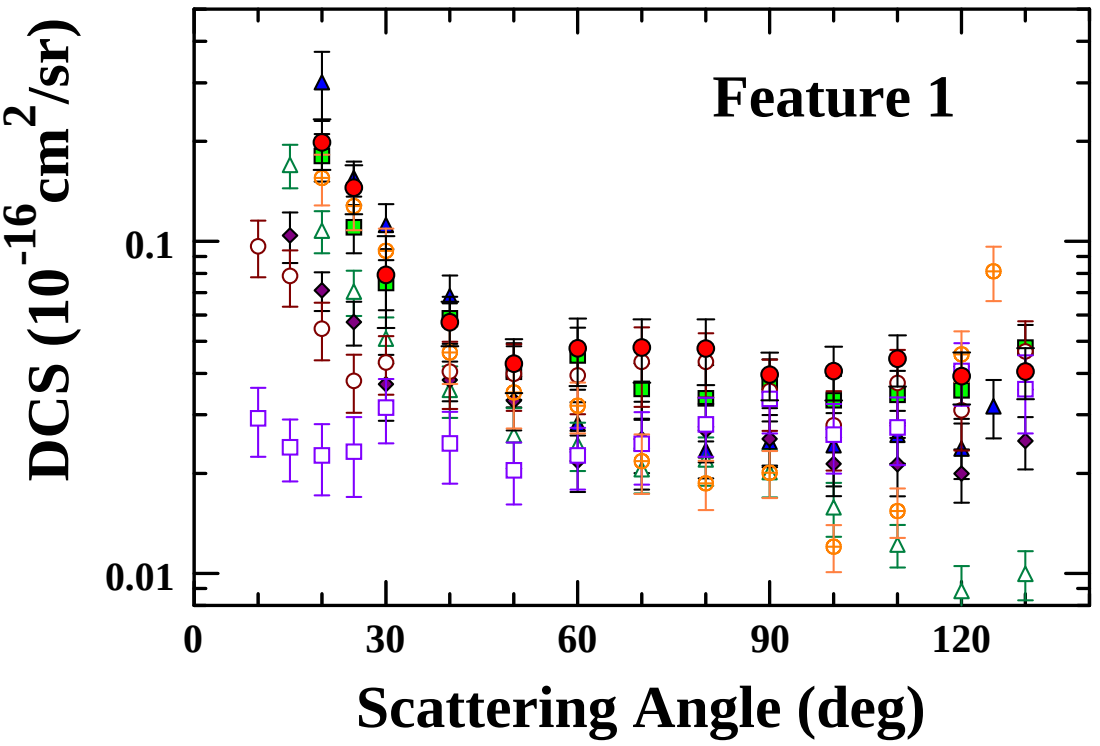
Feature 1
DCS (10^{-16} cm^2/sr)
0.1
0.01
0
30
60
90
120
Scattering Angle (deg)

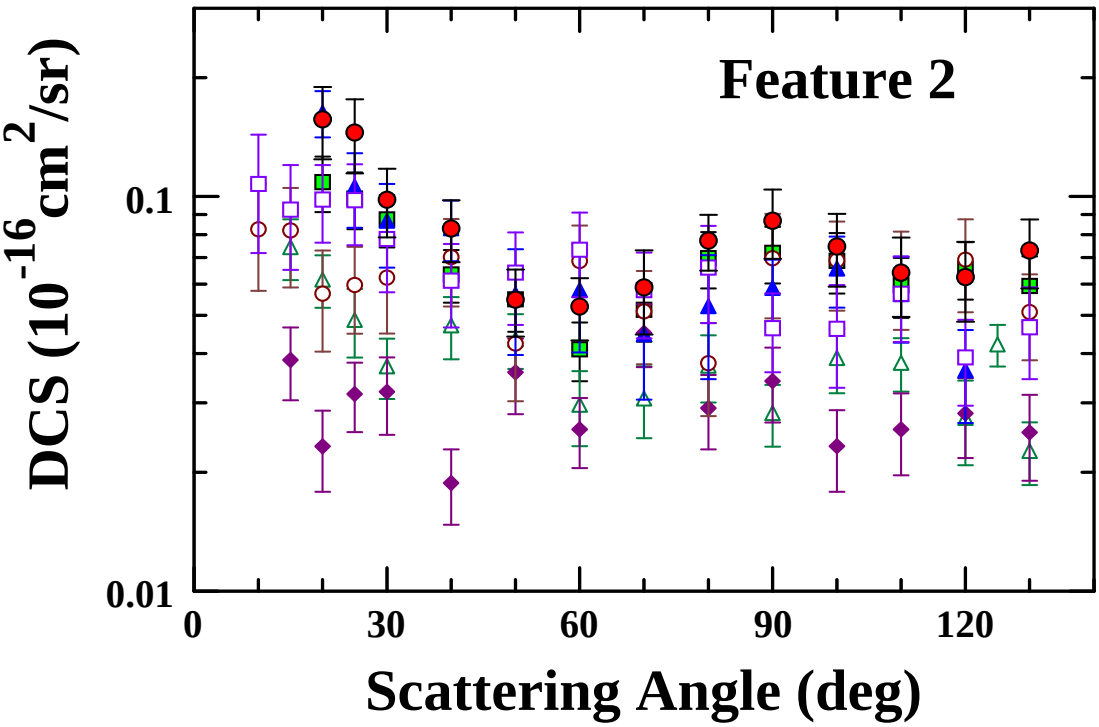
Feature 2
DCS (10^{-16} cm^2/sr)
0.1
0.01
0
30
60
90
120
Scattering Angle (deg)

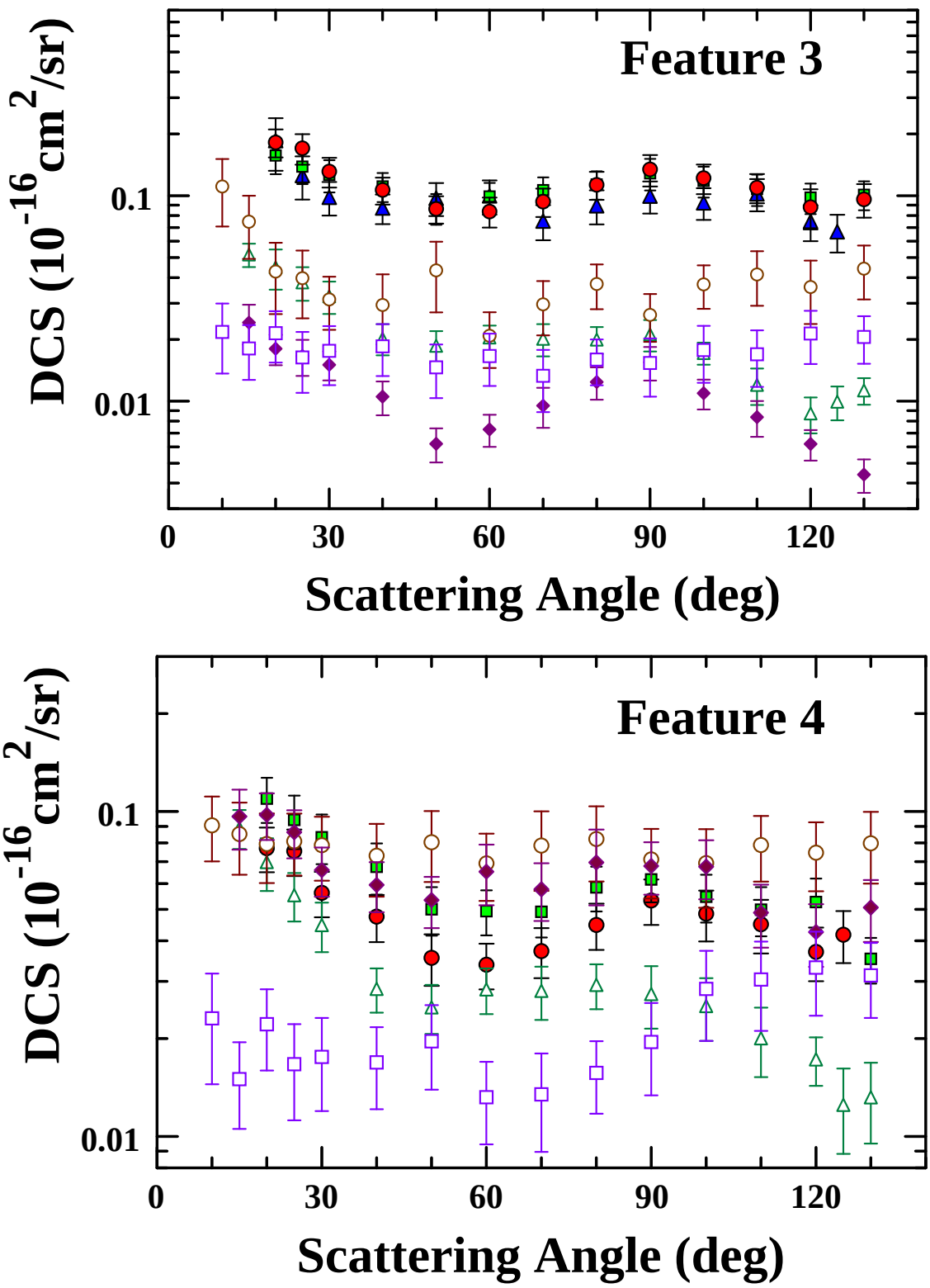

Figure 7 (Color online): Experimental DCSs for vibrational excitation of features for the feature specified in Table 2. Legend for E_0 values: ⊕ 1.25 eV, ▲ 1.5 eV, ● 1.75 eV, ■ 2.0 eV, △ 3.0 eV, ♦ 5.0 eV, O 8.0 eV and □ 15 eV. See text for discussion.

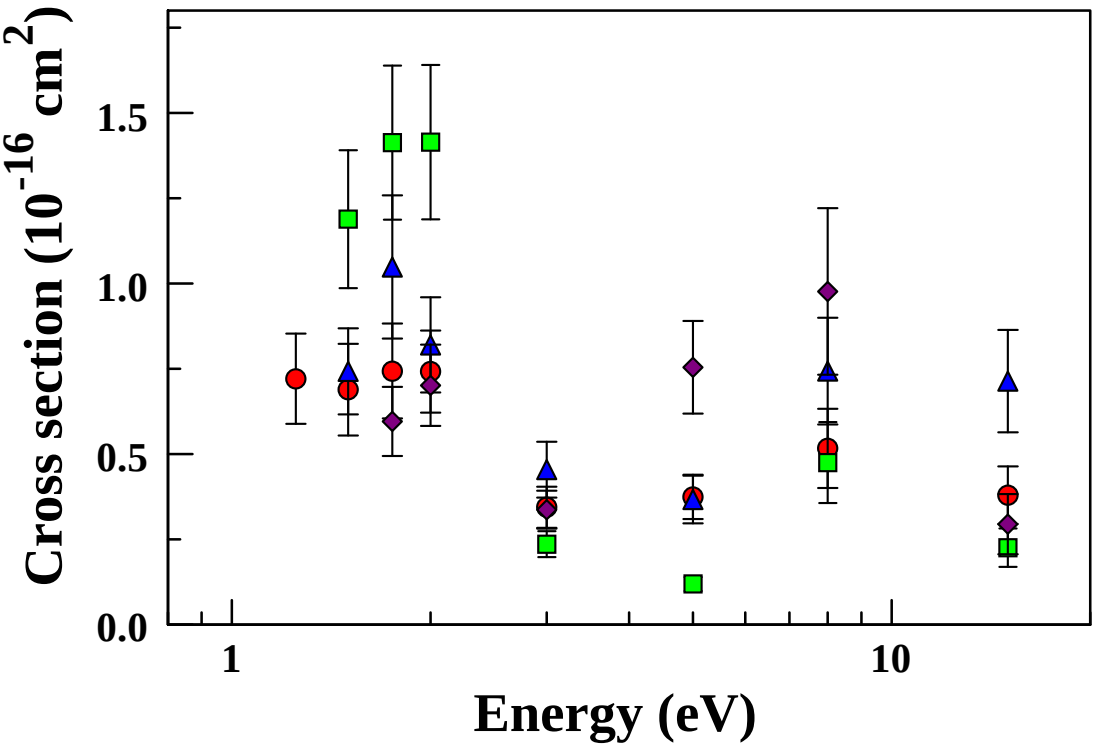

Figure 8 (Color online): Experimental ICSs for vibrational excitation of features specified in Table 1. Legend: ● Feature 1, ▲ Feature 2, ■ Feature 3, ♦ Feature 4. See text for discussion.